AGU PUBLICATIONS

JGR

Journal of Geophysical Research: Space Physics

RESEARCH ARTICLE
10.1002/2014JA019847

Key Points:
- Presents 2009 SSW effects on low-latitude ionospheric parameters over India
- Show strong semidiurnal and 16 day variations in E × B, EEJ, and F layer parameters
- Observed strong effects on E and F region irregularities, not reported before

Correspondence to:
A. K. Patra,
akpatra@narl.gov.in

Citation:
Patra, A. K., P. Pavan Chaitanya, S. Sripathi, and S. Alex (2014), Ionospheric variability over Indian low latitude linked with the 2009 sudden stratospheric warming, *J. Geophys. Res. Space Physics*, *119*, 4044–4061, doi:10.1002/2014JA019847.

Received 3 FEB 2014
Accepted 23 APR 2014
Accepted article online 29 APR 2014
Published online 27 MAY 2014

Ionospheric variability over Indian low latitude linked with the 2009 sudden stratospheric warming

A. K. Patra[1], P. Pavan Chaitanya[1], S. Sripathi[2], and S. Alex[2]

[1]National Atmospheric Research Laboratory, Gadanki, India, [2]Indian Institute of Geomagnetism, Navi Mumbai, India

Abstract In this paper, we analyze radar observations of **E** × **B** drift and plasma irregularities, ionosonde observations of *E* and *F* layer parameters including spread *F*, and magnetic field observations made from Indian low latitudes linked with the 2009 sudden stratospheric warming (SSW) event. **E** × **B** drift variations presented here are the first of their kind from the Indian sector as far as the effect of SSW is concerned. Difference of magnetic fields observed from the equator and low-latitude (ΔH) and **E** × **B** drift show linear relation, and both show remarkably large positive values in the morning and negative values in the afternoon exhibiting semidiurnal behavior. Remarkable changing patterns in the critical frequency of F_2 layer (f_oF_2) and F_3 layer (f_oF_3) were observed after the occurrence of SSW. Large variations with quasi 16 day periodicity were observed in ΔH, f_oF_2, and f_oF_3. Both semidiurnal and quasi 16 day wave modulation observed after the 2009 SSW event are consistent with those reported earlier. We also noted quasi 6 day variations in ΔH and f_oF_2 soon after the SSW commencement, not much reported before. During the counterelectrojet events linked with the SSW event, while equatorial E_s (E_{sq}) disappeared as expected, there were no blanketing E_s (E_{sb}), a finding not reported and discussed earlier. E_{sb} was also not formed at the off-equatorial location, indicating the absence of required vertical wind shear, but *E* region plasma irregularities were observed by the ionosonde and radar with a close relationship between the two. Weak *F* region irregularities were observed in the postmidnight hours, and case studies suggest the possible role of SSW-related background electric field in the manifestation of postmidnight *F* region irregularities.

1. Introduction

Understanding the quiet time ionospheric variability continues to be a challenging task and more so for the contemporary requirement of forecasting ionospheric weather for navigation and communication applications. Recent findings on unanticipated response of the midlatitude and low-latitude ionosphere-thermosphere system to the sudden stratospheric warming (SSW) has added a new dimension to the understanding of the quiet time ionospheric variability, an important component of the ionospheric weather forecasting [*Goncharenko and Zhang*, 2008; *Chau et al*., 2009, 2010]. SSW is a large-scale high-latitude stratospheric phenomenon characterized by a sudden (within a few days) deceleration/reversal of the zonal wind (eastward wind) of the polar vortex in the winter hemisphere and rise in stratospheric temperature by several tens of degrees. It is well known that the key mechanism for the onset of SSW is the growth of planetary scale waves propagating upward from the troposphere and their nonlinear interaction with the zonal mean flow [*Matsuno*, 1971].

Given the fact that SSW can be predicted a few days in advance [*Kim and Flatau*, 2010], it provides an opportunity to develop and test forecasting skill of the low-latitude ionosphere. The observed differences in the longitudinal responses [e.g., *Vineeth et al*., 2009; *Sridharan et al*., 2009; *Anderson and Araujo-Pradere*, 2010; *Fejer et al*., 2010], however, make forecasting as challenging as it was before. Moreover, the response of the low-latitude ionosphere at a given longitude also varies from one SSW event to another [e.g., *Sathishkumar and Sridharan*, 2009; *Fejer et al*., 2010]. A comprehensive review on the response of the low- and midlatitude ionosphere to SSW can be found in *Chau et al*. [2012]. Since then several research papers, showing low-latitude and midlatitude ionospheric variabilities at time scales of gravity wave, tide, and planetary wave in association with SSW activity, have appeared [*Rodrigues et al*., 2011; *Sathishkumar and Sridharan*, 2011, 2013; *Sripathi and Bhattacharyya*, 2012; *Upadhayaya and Mahajan*, 2013].

Numerical modeling studies have also been performed to reproduce SSW-associated changes in ionospheric parameters and to examine the possible underlying physical mechanisms [e.g., *Fuller-Rowell et al*., 2010;

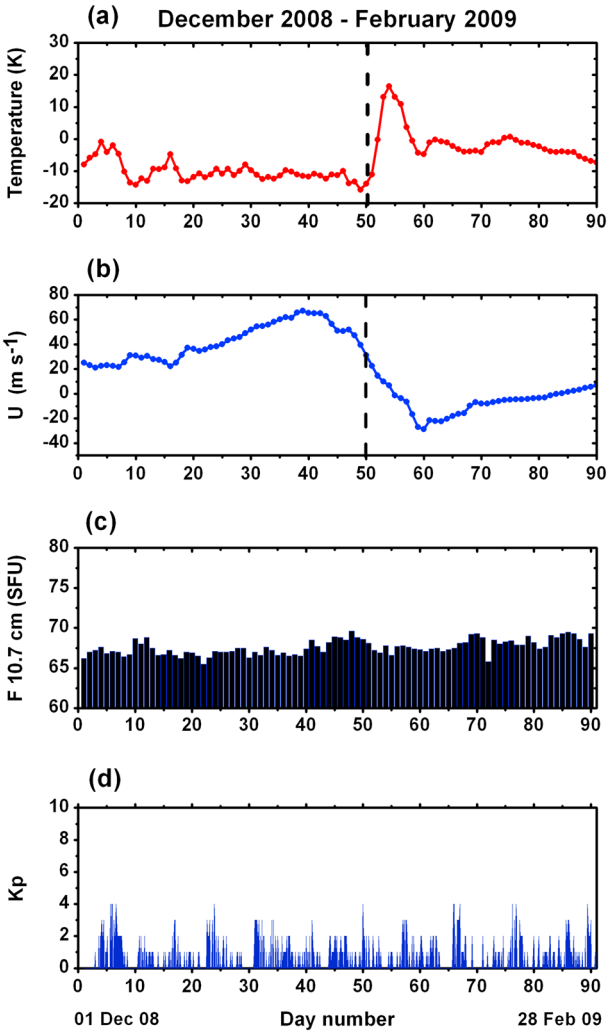

Figure 1. Summary of the 2009 SSW displaying (a) zonal mean temperature difference of 90°N and 60°N latitudes at 10 hPa (32 km) and (b) zonal mean wind at 60°N latitude at 10 hPa (32 km), and solar and magnetic activities in terms of (c) radio flux at 10.7 cm ($F_{10.7cm}$) and (d) *Kp* index during the period December 2008 to February 2009. The vertical dashed lines in Figures 1a and 1b represent the onset of SSW.

Wang et al., 2011; *Fang et al.*, 2012; *Forbes and Zhang*, 2012; *Jin et al.*, 2012; *Pedatella and Liu*, 2013; *Liu et al.*, 2013; *Maute et al.*, 2014]. A clear picture on SSW effects on the ionosphere, however, has yet to emerge.

In this paper, we provide new observational knowledge on the ionospheric changes linked with the SSW event of 2009 based on a comprehensive multiparameter data set of the equatorial and low-latitude ionosphere from the Indian longitude sector. We use radar observations of **E** × **B** drifts, ionosonde observations of *E* and *F* layer parameters, and equatorial low-latitude magnetic field observations to characterize ionospheric variations. The **E** × **B** drifts, which were estimated using daytime 150 km echoes, reported here are unique since such data from equatorial latitude linked with SSW have so far been reported only from Jicamarca. We also use radar and ionosonde observations to study the characteristics of the *E* and *F* region irregularities linked with the SSW event of 2009.

2. Description of the 2009 SSW Event and Observations

The SSW event of 2009 was the strongest and most prolonged event ever recorded [*Manney et al.*, 2009]. Figures 1a and 1b provide the characteristic features of the 2009 SSW event in terms of zonal mean temperature difference of 90°N and 60°N latitudes and zonal mean zonal wind at 60°N latitude both at 10 hPa (~32 km), respectively. Temperature difference and zonal wind, presented in Figures 1a and 1b, have been taken from the website of National Centers for Environmental Prediction (NCEP). The event commenced on 19 January (day number 50, represented by vertical dashed line); peak warming occurred on 23 January (day number 54); subsequently, warming decreased noticeably by 29 January (day number 60), and temperature became moderate afterward. Magnitude of eastward wind decreased substantially on 19 January (day number 50) and the reversal from eastward to westward coincided well with the day of the peak warming (i.e., 23 January). Figures 1c and 1d show radio flux at a wavelength of 10.7 cm ($F_{10.7cm}$) as a measure of solar activity and K_p index as a measure of magnetic activity, respectively. As is evident from these figures the period of 2009 SSW is characterized by extremely low solar activity and persisting magnetically quiet conditions and thus is well suited for studying the low-latitude ionospheric response to SSW.

To study the ionospheric changes linked with the 2009 SSW, we use radar observations of **E** × **B** drifts and ionosonde observations of *E* and *F* region parameters from Gadanki (13.5°N, 79.2°E, dip latitude 6.5°), ionosonde and magnetometer observations from Tirunelveli (8.7°N, 77.8°E, dip latitude 0.4°N), a magnetic

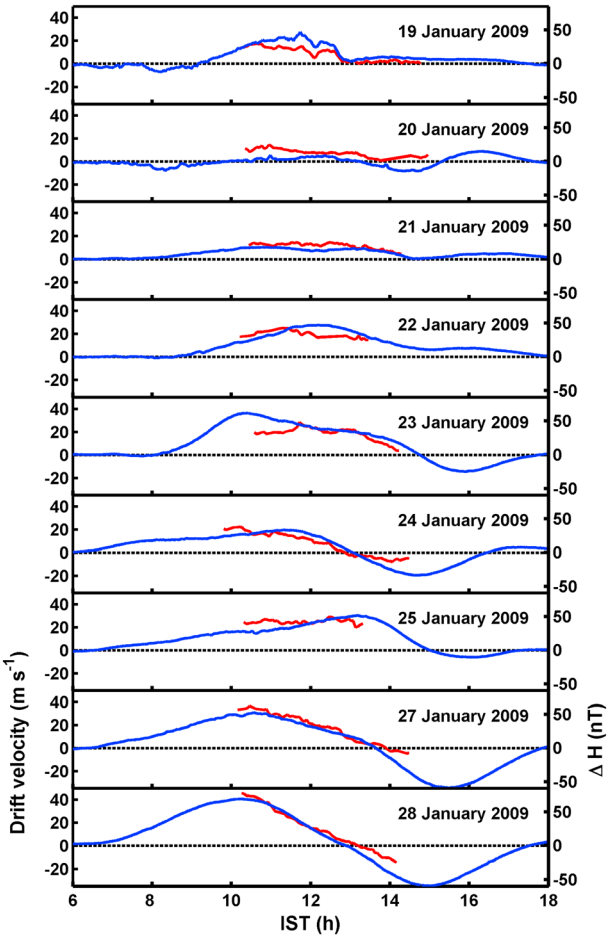

Figure 2. Daytime **E** × **B** drifts as a function of time estimated using the mean Doppler shift of 150 km echoes during 19–28 January 2009 (except for 26 January) are shown in red lines. Time variation of ΔH ($\Delta H_{\text{Tirunelveli}} - \Delta H_{\text{Alibag}}$), representing variation in the daytime electrojet strength, during the same period are also shown as blue lines. Note that the scales for **E** × **B** drift and ΔH are given on the left and right, respectively.

equatorial location, and magnetometer observations from Alibag (18.5°N, 72.9°E, dip latitude 13.0°N), a location well beyond the electrojet belt.

E × **B** drifts were derived using the daytime 150 km echoes made using the 53 MHz mesosphere-stratosphere-troposphere (MST) radar located at Gadanki. Details on the radar experiments of 150 km echoes, and related data processing methods have been described earlier by *Patra et al.* [2012]. Radar observations were made during 19–28 January 2009, except on 26 January 2009, when the SSW activity was at the peak. Observations were also made during 17–27 February 2009, except on 24 and 25 February 2009 when SSW activity subsided. Daytime 150 km echoes were observed during 9:30–14:00 IST on all the days. Unfortunately, we did not conduct observations in December 2008 to examine the **E** × **B** drifts prior to the SSW event. In order to compare the **E** × **B** drifts during SSW and after SSW with those of non-SSW period, we use observations made during 10–24 December 2009. During this period, however, observations were not made during 12–17 December and 21 December due to other experimental schedule of the Gadanki MST radar.

Ionosonde observations have been used to characterize the F_2 and F_3 layers, sporadic *E* layer, and spread *F*. Much of the observations, however, correspond to Gadanki, which have been used to carry out a detailed study on the variability in electron density of the F_2 and F_3 layers in terms of f_oF_2 and f_oF_3. A few days of ionosonde observations from Gadanki and Tirunelveli have also been used to examine the characteristics of the *E* region and also equatorial spread *F*.

We use magnetic field observations from Tirunelveli and Alibag and utilize ΔH (i.e., $\Delta H_{\text{Tirunelveli}} - \Delta H_{\text{Alibag}}$) to characterize the electrojet/counterelectrojet and associated variabilities. It may be mentioned that the difference of horizontal magnetic fields measured from a pair of stations, one located at the magnetic equator and another from low latitude, provides a measure of the daytime integrated electrojet current [*Rastogi and Klobuchar*, 1990] and is being used as a proxy of zonal electric field [e.g., *Anderson et al.*, 2002].

3. Observational Results

3.1. E × B Drift and ΔH

3.1.1. Observations During the SSW

E × **B** drifts were observed during 19–28 January 2009, except on 26 January. **E** × **B** drifts and corresponding ΔH ($\Delta H_{\text{Tirunelveli}} - \Delta H_{\text{Alibag}}$) values, representing variation in the daytime electrojet strength, as a function of time are presented in Figure 2 (top to bottom). The red lines represent **E** × **B** drifts with a scale marked on the left, and the blue lines represent ΔH values with a scale marked on the right. While the **E** × **B** drifts are

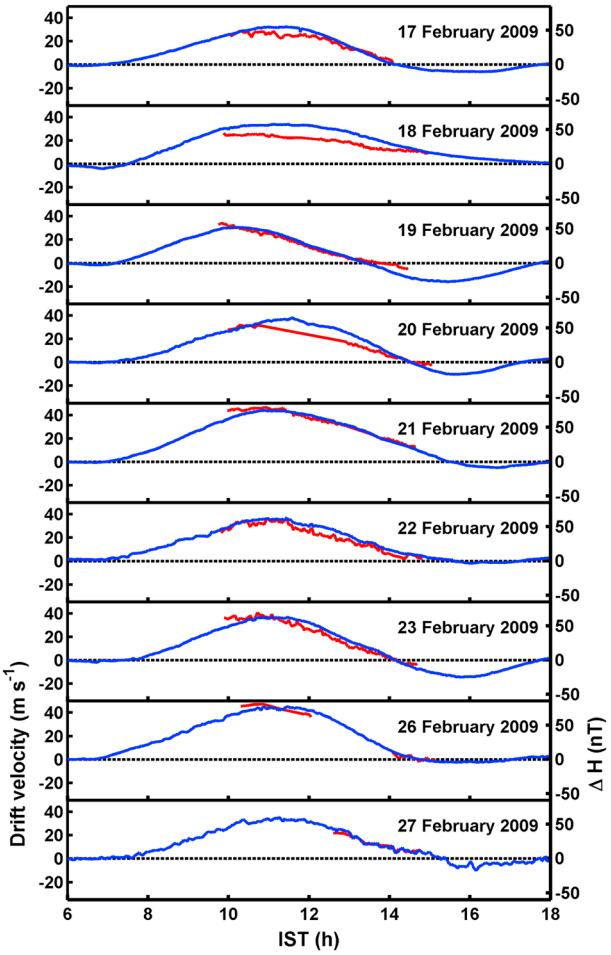

Figure 3. Same as Figure 2 but for the period of 17–27 February 2009.

mostly positive, representing eastward electric field, near-zero or negative drifts were observed in the afternoon hours except for 22 and 25 January. Negative drifts were clearly observed on 24, 27, and 28 January and out of these days, large positive drifts in the morning hours were observed on 27 and 28 January. Further, out of these 2 days (27 and 28 January), the velocity reversal was rather fast on 28 January. The local times at which electric field reversals occurred were also different: on 23, 24, 27, and 28 January the reversal times were 14:15, 13:00, 13:45, and 13:00 IST, respectively. As can be noted from ΔH variations, electrojet was completely suppressed on 20 January and was weak on 21 January. On these days, although $\mathbf{E} \times \mathbf{B}$ drifts were smaller than those observed on other days, they were all positive, indicating the presence of eastward electric field. Given the fact that zonal electric field was eastward and ΔH was close to zero on 20 January, it is quite likely that an additional westward current sheet, presumably due to height varying wind, was present on that day. Counterelectrojet activity was observed on every day afternoon after 23 January, and the counterelectrojet was strong on 27 and 28 January with magnetic field as high as −60 nT. The period of negative excursion varied from 2 to 5 hours and showed nearly semidiurnal variation on 27 and 28 January. On 23 and 25 January counterelectrojet started nearly 1 hour later than the rest of the days. It is interesting to note that the times of the electrojet reversal were also 14:45, 13:00, 15:00, 13:45, and 13:00 IST on 23, 24, 25, 27, and 28 January, which are identical to those in the $\mathbf{E} \times \mathbf{B}$ drift. On 25 January ΔH gradually increased until 13 IST unlike other days, and $\mathbf{E} \times \mathbf{B}$ drifts also showed similar behavior. All these clearly indicate a close relationship between the zonal electric field and electrojet strength.

3.1.2. Observations After the SSW

$\mathbf{E} \times \mathbf{B}$ drifts were observed during 17–27 February 2009, except on 24 and 25 February 2009. $\mathbf{E} \times \mathbf{B}$ drifts and corresponding ΔH values observed on these days are presented in Figure 3 in the same way as those shown in Figure 2. While $\mathbf{E} \times \mathbf{B}$ drifts were mostly positive, indicating eastward electric field, there was clear indication of velocity reversal on several days at ~14 IST. The reversal of $\mathbf{E} \times \mathbf{B}$ drifts is found to be associated with counterelectrojet activity, although the strength of counterelectrojet was much weaker than those observed on 27–28 January 2009. In fact, negative velocities, representing westward electric field, were clearly observed on 19 February and 23 February when counterelectrojet activity was stronger than the rest of the days. Again, in these observations, a close relationship between $\mathbf{E} \times \mathbf{B}$ drifts and ΔH is noticed.

3.1.3. Observations During Non-SSW Period

In order to study $\mathbf{E} \times \mathbf{B}$ drifts and ΔH variations during the Northern Hemisphere winter but for non-SSW period, we present observations made during 10–24 December 2009 in Figure 4 in the same way as those shown in Figure 2. Note that observations were not made during 12–17 December and 21 December. Gaps in the $\mathbf{E} \times \mathbf{B}$ drift data are due to poor signal-to-noise ratio of 150 km echoes. Note that afternoon counterelectrojet activity was not observed, and $\mathbf{E} \times \mathbf{B}$ drifts were also positive including those observed

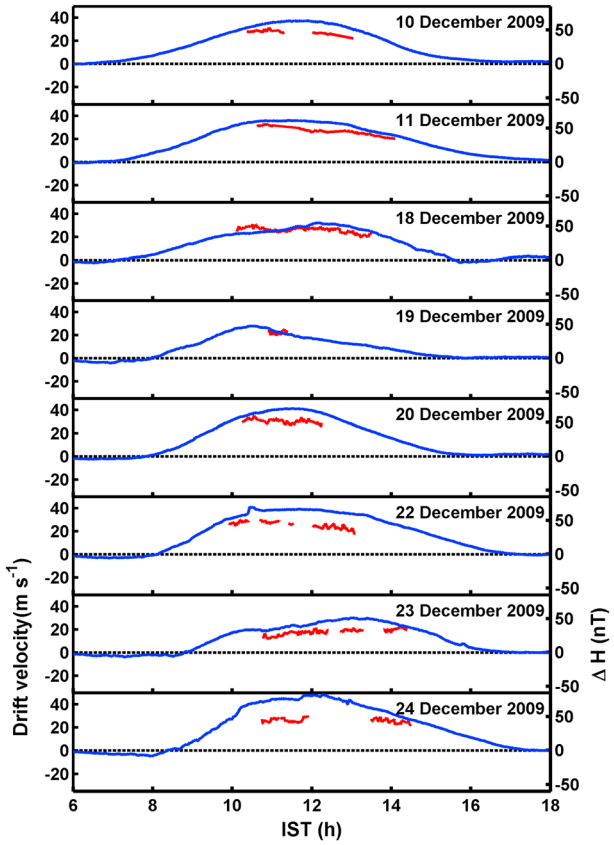

Figure 4. Same as Figure 2 but for the period of 10–24 December 2009.

after 14 IST. These observations are in contrast to those shown in Figures 2 and 3, which were made during SSW and after SSW.

To demonstrate the relationship between $\mathbf{E} \times \mathbf{B}$ drift and ΔH shown in Figures 2–4, we present scatterplots of these parameters in Figures 5a–5c, respectively. Figure 5 clearly suggests a linear relationship between $\mathbf{E} \times \mathbf{B}$ drift and ΔH with correlation coefficients varying between 0.85 and 0.95, implying that electrojet observations can be suitably modeled to derive zonal electric field consistent with the finding of *Anderson et al*. [2002]. Estimation of electric field, however, is beyond the scope of this paper, and this exercise will be taken up in a separate study using a larger database than that used here. Instead, we will use a sufficiently long data set of ΔH here to study the variabilities in the electrojet and also in zonal electric field as a proxy.

In order to examine the variabilities in the electrojet (also in zonal electric field), we present daytime variation in ΔH as a function of day number during the period December 2008 to February 2009 in Figure 6a. Two discrete periods of afternoon counterelectrojet are very much apparent in this figure. The first one occurred during 23–31 January (day numbers 54–62), and the second one occurred after 8 days beginning from 8 February (day number 70), which was intense during 8–14 February (day numbers 70–76) and subsequently decreased in strength. It is also interesting to note a similar stretch of strong forenoon electrojet, but it was delayed by 3 days with respect to the first stretch of the counterelectrojet events. Subsequently, the strength of the forenoon electrojet subsided for a period of ~7 days, which is very similar to the gap between the first and second stretch of the counterelectrojet events. Further, ΔH variations after 23 January (day number 54) are characterized by forenoon electrojet and afternoon counterelectrojet showing a clear semidiurnal pattern. After 12 February (day number 74), however, counterelectrojet was weaker than that observed prior to 12 February.

To examine planetary scale variability in the electrojet, if any, we performed wavelet analysis on ΔH values observed at 10 IST and 16 IST. Figures 6b and 6c show the time series of ΔH and its wavelet spectrum corresponding to 10 IST, respectively. Similarly, Figures 5d and 5e show results corresponding 16 IST. In Figures 6c and 6e, a dominant period of ~15 days peaking around 23 January (day number 54) can be noted. In addition to this, at 10 IST we note an additional period of ~6 days. Interestingly, both 15 day and 6 day periods are found to be the strongest during the period when the SSW was at the peak. The effect of 15 day period, however, lasted longer than that of 6 day period.

3.2. Variabilities in F_2 Layer and F_3 Layer Peak Plasma Frequencies

Figures 7a and 7b show peak plasma frequency of F_2 layer (f_oF_2) and F_3 layer (f_oF_3), respectively, observed at Gadanki during December 2008 to February 2009. As can be noted from Figure 7a, f_oF_2 did not show much variation with time as well as day number until the beginning of January, showed smaller values during 12–16 IST than those observed prior to 12 IST and after 16 IST until 23 January (day number 54) and showed much variation both with time and day number after 23 January (day number 54) until 12 February (day number 74). After 23 January (day number 54), f_oF_2 values were remarkably larger in the afternoon hours,

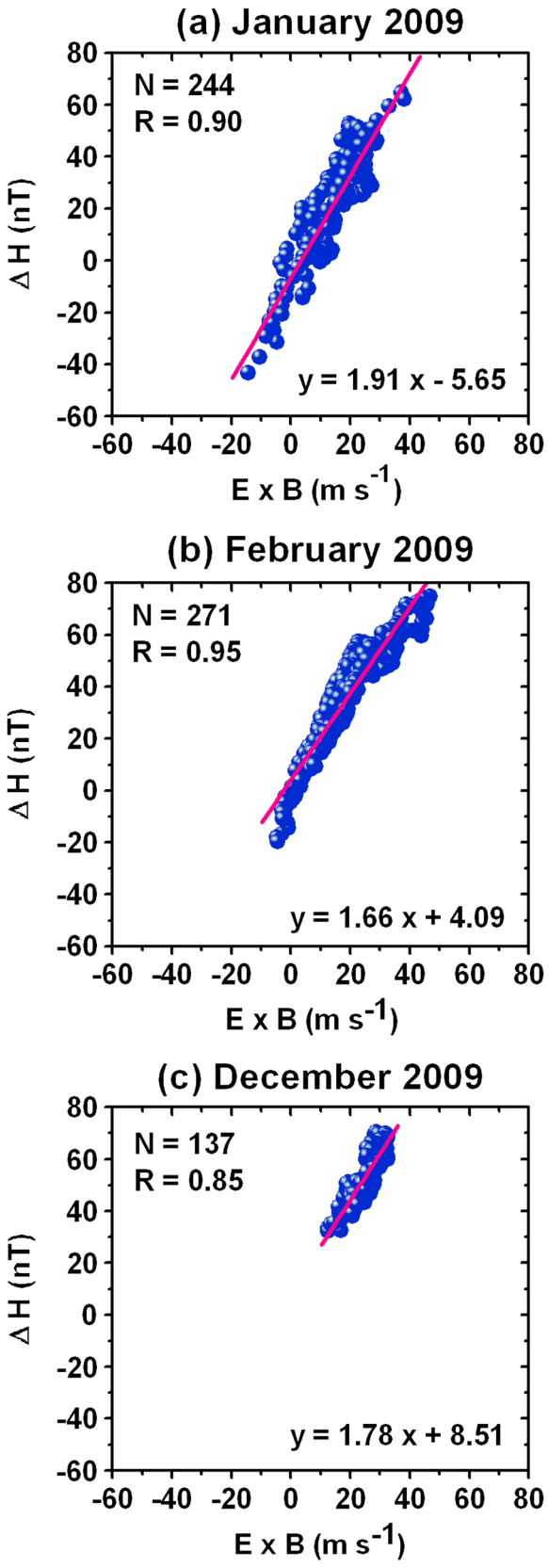

Figure 5. Scatterplot of **E** × **B** and Δ*H*, observed during (a) 19–28 January, (b) 17–27 February, and (c) 10–24 December 2009, illustrating the relationship between these parameters. In each figure, *N* and *R* represent number of data points and cross-correlation coefficient, respectively. A linear fit equation is also shown in each figure.

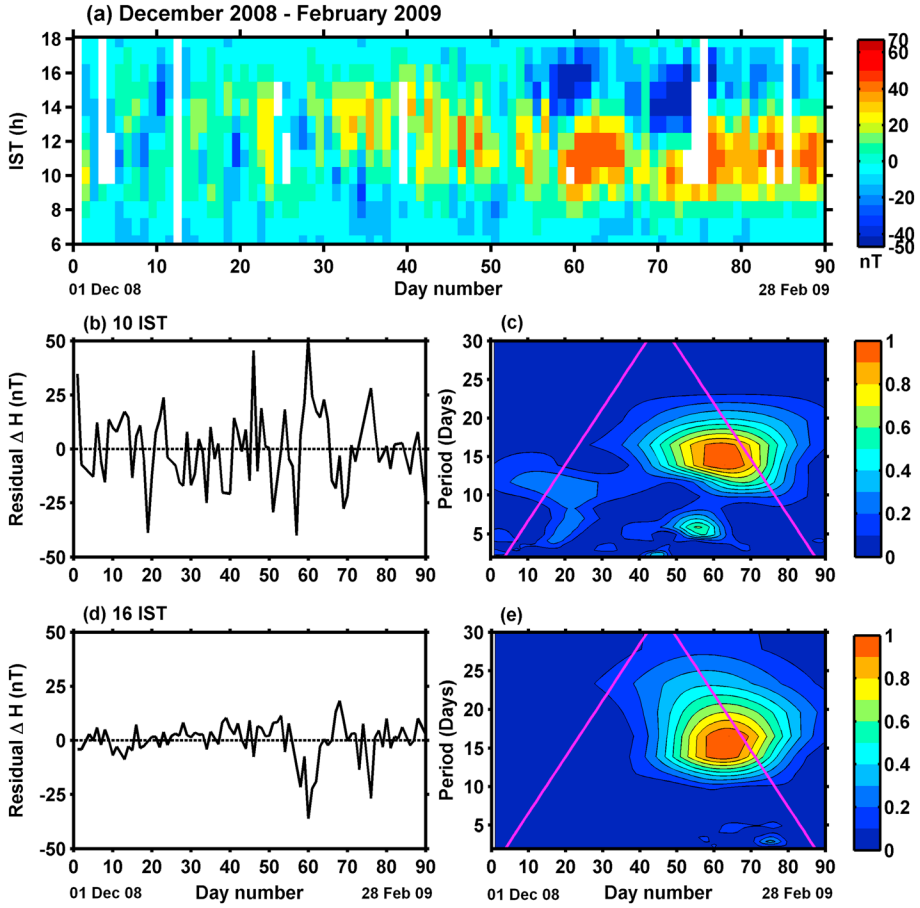

Figure 6. (a) Daytime variation of Δ*H* during December 2008 to February 2009, (b) variation of Δ*H* as a function of day number observed at 10 IST, (c) wavelet spectrum displaying the dominant periods in Δ*H* observed at 10 IST as a function of day number, (d) variation of Δ*H* as a function of day number observed at 16 IST, and (e) wavelet spectrum displaying the dominant periods in Δ*H* observed at 16 IST as a function of day number.

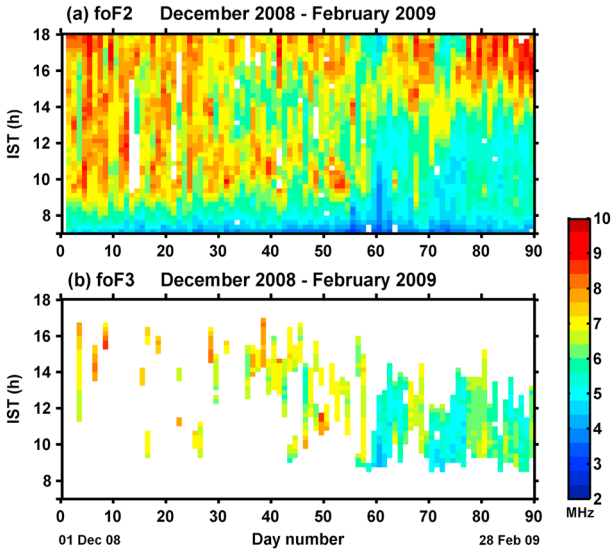

Figure 7. Daytime variations in (a) f_oF_2 and (b) f_oF_3 as a function of day number observed at Gadanki during December 2008 to February 2009.

especially after 14 IST, than those in the forenoon. This variation resembles semidiurnal variation observed in Δ*H* data. Notably, during this period and prior to 14 IST, f_oF_2 values were very small compared to those observed before 23 January (day number 54). During this time and period F_3 layers were observed, and f_oF_3 showed remarkable variation with periods of about 15 days. A noteworthy observation is the low values of f_oF_2 during 16–18 IST around day numbers 60 and 75 and their close association with the strong afternoon counterelectrojet (shown in Figure 6) observed on those days. The low values of f_oF_2, however, were observed after about an hour of the counterelectrojet events.

Figure 7b illustrates interesting aspects of the F_3 layer in terms of its occurrence and f_oF_3. These changing patterns can be noted

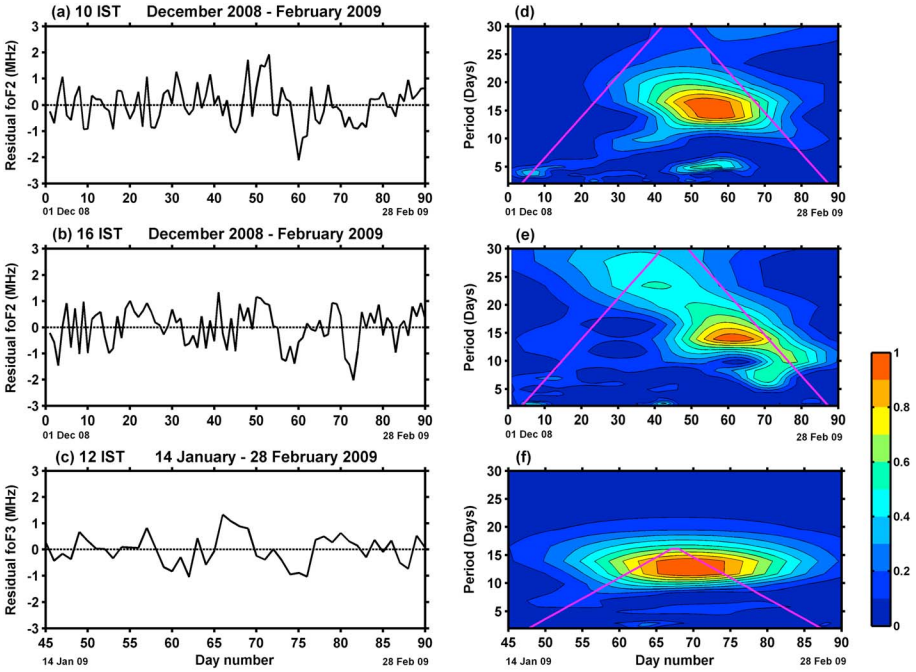

Figure 8. Variation of f_oF_2 observed at (a) 10 IST and (b) 16 IST and (c) f_oF_3 observed at 12 IST as a function of day number. Wavelet spectrum of f_oF_2 corresponding to the observations at (d) 10 IST and (e) 16 IST and f_oF_3 (f) corresponding to the observations at 12 IST as a function of day number. In case of f_oF_3, observations made since 14 January (day number 45) have been used since F_3 layer was observed regularly only after 14 January.

from the later part of January, which continued until the first half of February. During December–January, occurrence of the F_3 layer was sporadic and spread over a long time duration, while in February occurrence of the F_3 layer was quite regular and mostly confined to 9–14 IST. Further, f_oF_3 was found to have similar pattern as that of f_oF_2 (with periods of about 15 days), but F_3 layer occurred during those days and times when f_oF_2 was very low.

Figure 8 shows time evolution of planetary scale variability obtained using wavelet analysis performed on f_oF_2 and f_oF_3. In case of f_oF_3, however, we have used observations since 14 January (day number 45) since F_3 layer was observed regularly only after 14 January. Figures 8a and 8b show time series of f_oF_2 observed at 10 IST and 16 IST, respectively, and Figure 8c shows f_oF_3 observed at 12 IST. Wavelet spectrum of f_oF_2 and f_oF_3, corresponding to those presented in Figures 8a–8c, are shown in Figures 7d–7f, respectively. Wavelet spectra of f_oF_2 both at 10 IST and 16 IST show dominant period of 15 days peaking around 23 January (day number 54). Presence of a secondary period of ~6 days can also be noted in the 10 IST observations. In addition to these, observations made at 16 IST reveal a period of 23 days occurring around 10 January (day number 41) and a period of 7 days occurring around 10 February (day number 72). Strong variation with periodicity of 13 days can also be noted in f_oF_3 after 19 January (day number 50), the date of SSW commencement. It may be recalled (from Figure 6) that a dominant period of 15 days and secondary period of 6 days peaking around 23 January (day number 54) was also noted in ΔH observations.

3.3. *E* Region Characteristics at and off the Magnetic Equator

Disappearance of equatorial E_s (E_{sq}) or occurrence of blanketing E_s (E_{sb}) has been observed in association with counterelectrojet event [e.g., *Bhargava and Subrahmanyan*, 1964; *Rastogi*, 1972]. At the magnetic equator, while the disappearance of E_{sq} has been well understood with the reversal of vertical electric field (which also manifest counterelectrojet), occurrence of E_{sb} has not been understood yet [*Tsunoda*, 2008]. Given the fact that the wind shear theory [*Axford*, 1963] is not effective in forming ion layers at the magnetic equator, meridional transport of metallic ion-dominated E_s layer has been invoked to account for the occurrence of dip equatorial E_{sb} [*Reddy and Devasia*, 1973; *Chandra and Rastogi*, 1975]. It is also not clear whether the

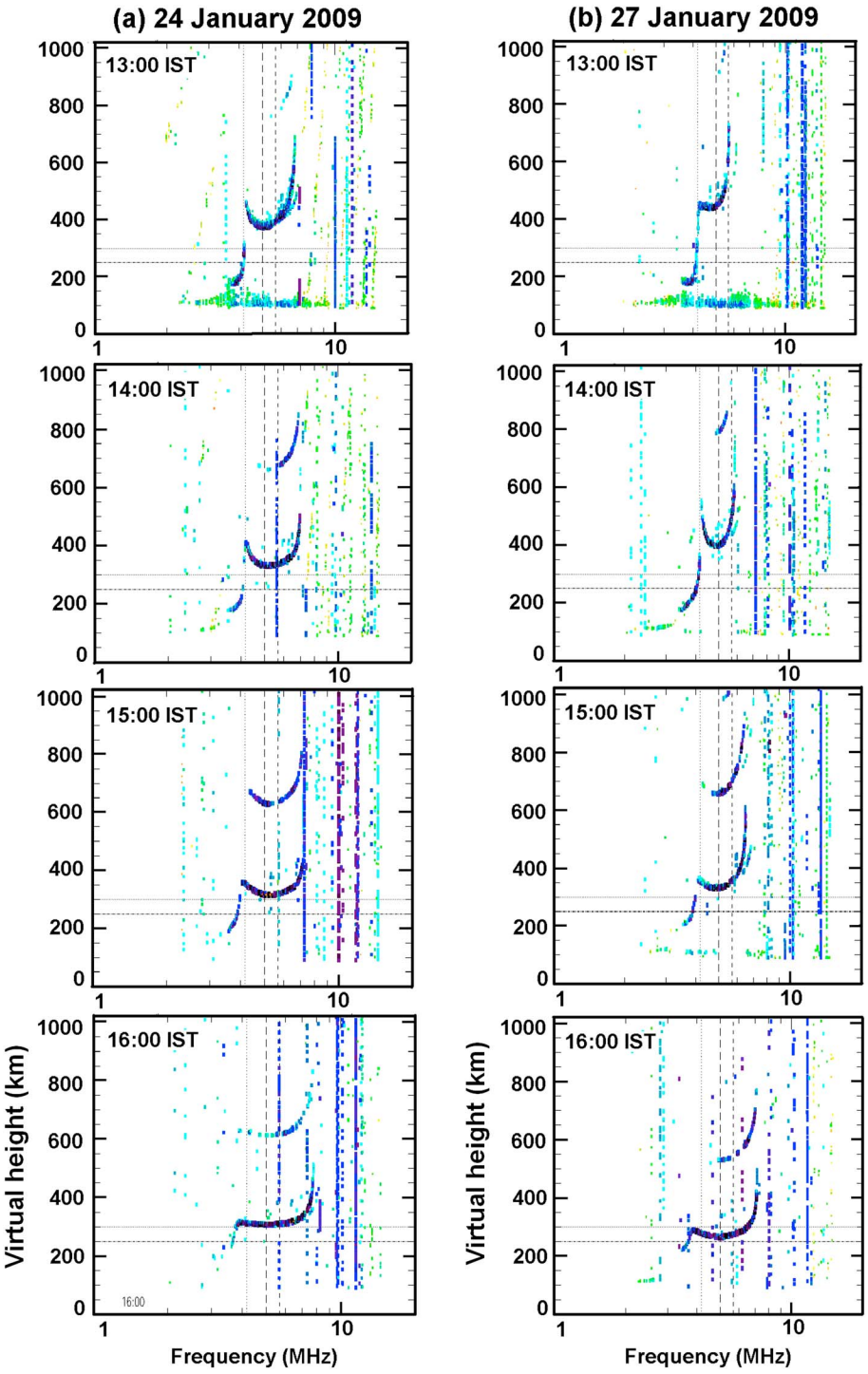

Figure 9. Ionograms observed at Tirunelveli at (top to bottom) 13–16 IST on (a) 24 January 2009 and (b) 27 January 2009. Note that E_{sq} disappeared after 14 IST, but no E_{sb} was observed.

occurrence of E_{sb} at the magnetic equator is dependent on the strength of counterelectrojet [e.g., *Devasia et al.*, 2004].

In order to examine the characteristics of the *E* regions at and off the equator during the counterelectrojet events linked with the 2009 SSW event, we examine a few ionograms observed at Tirunelveli (equatorial station) and at Gadanki (off-equatorial station) in connection with two counterelectrojet events linked with

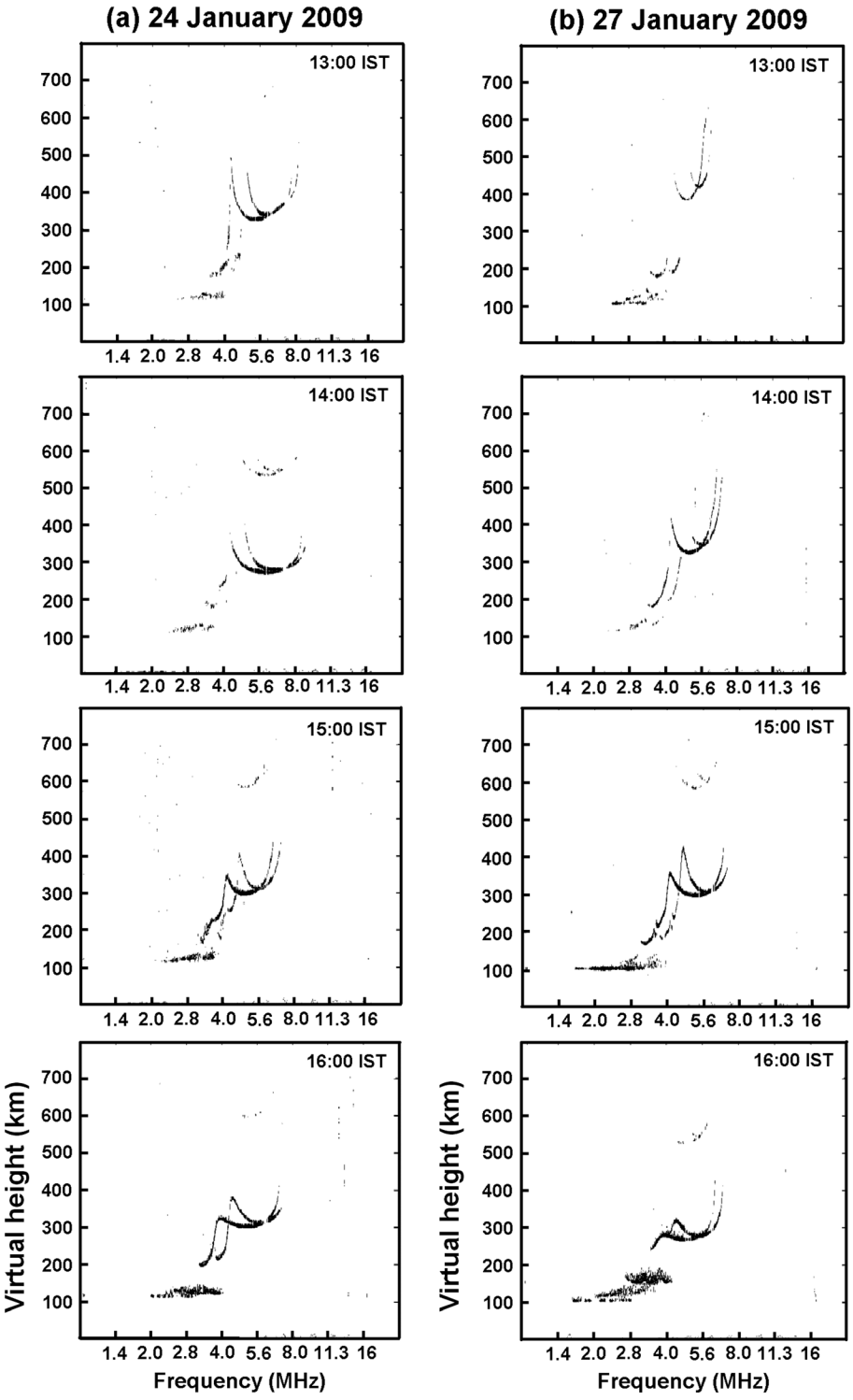

Figure 10. Same as Figure 8 but for observations from Gadanki. Ionograms display occurrence of E_s layers.

the 2009 SSW event. At the off-equatorial location, although we do not expect similar effects as at the magnetic equator, off-equatorial observations would provide vital information on the E_s characteristics, if any, to help understand the equatorward transport of E_{sb} invoked earlier to account for the occurrence of E_{sb} at the magnetic equator [*Reddy and Devasia*, 1973; *Chandra and Rastogi*, 1975]. In addition, off-equatorial

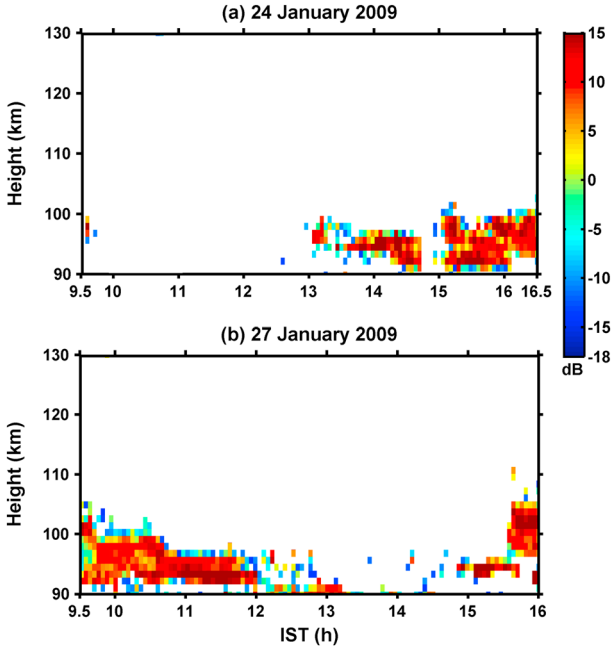

Figure 11. Height-time variations of signal-to-noise ratio of radar echoes from the *E* region field-aligned irregularities observed at Gadanki on (a) 24 January 2009 and (b) 27 January 2009.

observations would provide information on whether conditions necessary for the formation of low-latitude E_{sb} was induced by SSW.

During 20 January to 15 February, E_{sb} was observed only on 2, 5, 12, and 14 February. It may be recalled from Figure 6 that during these days counterelectrojet was either weak or not observed. In order to show the state of the *E* region, we show four selected ionograms observed at Tirunelveli during the counterelectrojet events of 24 and 27 January in Figures 9a and 9b, respectively. It may be mentioned that on both the days, E_{sq}-type echoes, representing Bragg scattering of radio waves from the electrojet irregularities, were present prior to the occurrence of counterelectrojet. In fact, at 13 IST also, when the electrojet current was either close to zero or slightly negative, ionograms can be characterized as E_{sq} type. Subsequently, at 14, 15, and 16 IST, no *E* region echo, either E_{sq} or E_{sb} type, was observed on both the days. It may be recalled from Figure 2 that on 24 and 27 January, counterelectrojet events were characterized with peak ΔH of -35 nT and -60 nT, respectively. Also zonal electric fields were westward during the counterelectrojet events (shown in Figure 2). Thus, the disappearance of E_{sq} and occurrence of counterelectrojet, both signify the presence of downward electric field and westward electric field, consistent with our understanding of the electrojet physics. What is noteworthy is the nonoccurrence of E_{sb} on these 2 days as well as on other days (not presented here) despite the fact that ΔH varied from near zero to as high as -60 nT.

In order to gain some insight on the possible equatorward transport of E_{sb}, we present a few ionograms observed at Gadanki during the counterelectrojet events of 24 and 27 January in Figures 10a and 10b, respectively. *E* region echoes can be characterized as normal *E* layer trace with no E_s activity at 13 IST and 14 IST, which turned into E_s type at 15 IST and 16 IST. We, however, noted intermittent occurrence of E_{sb} during 15–20 IST on both days (not shown), having second reflection but not blanketing the *F* layer significantly. Also, while we did not observe E_s during daytime on 24 January, intermittent occurrence of E_s was observed on 27 January. Although the overall occurrence of E_s on 27 January was higher than that of 24 January, strong E_{sb} was not observed on both the days.

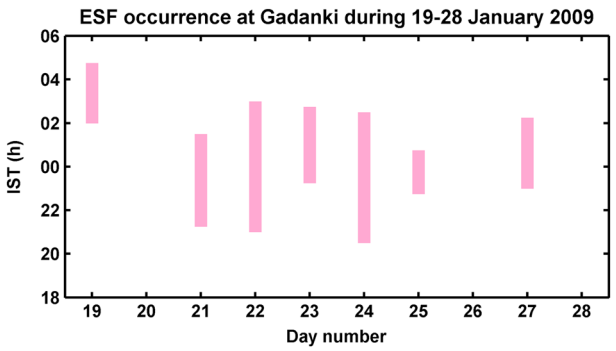

Figure 12. Duration of spread *F* occurrence based on ionosonde observations at Gadanki during 19–28 January 2009. The bars represent the occurrence duration of spread *F* (both range- and frequency-type spread *F*).

To characterize the low-latitude *E* region over Gadanki further, we present height-time variation of radar echoes from the *E* region field-aligned irregularities (FAI) observed on 24 and 27 January in Figures 11a and 11b, respectively. Radar echoes were not observed during 10–13 IST on 24 January and during 13:15–14:15 IST on 27 January. When we compared the radar observations with the collocated ionosonde observations, we found that the radar echoes were fairly correlated with the presence and type of E_s echoes (shown in Figure 10).

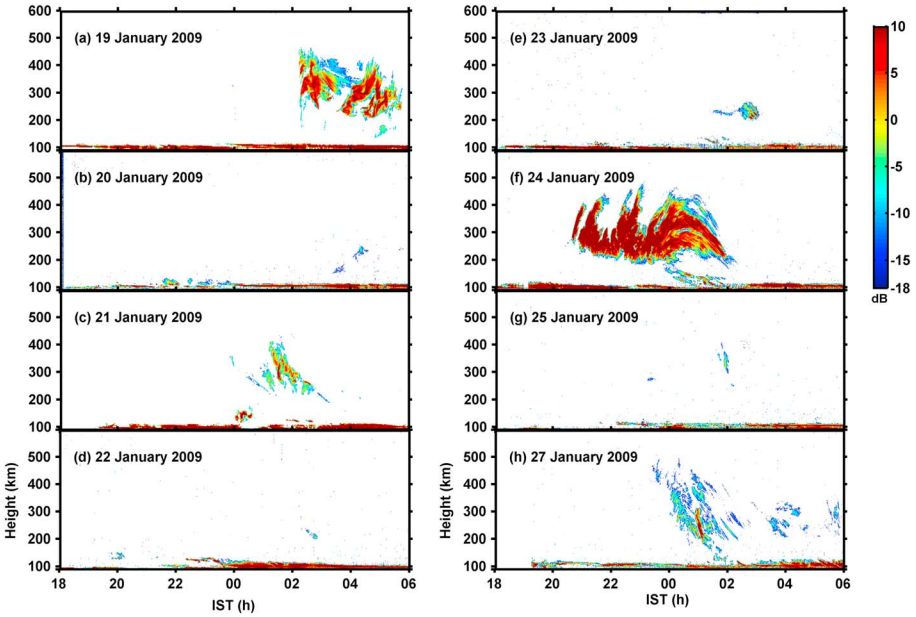

Figure 13. Height-time variations of signal-to-noise ratio of radar echoes from the *F* region field-aligned irregularities observed at Gadanki on (a) 19 January, (b) 20 January, (c) 21 January, (d) 22 January, (e) 23 January, (f) 24 January, (g) 25 January, and (h) 27 January 2009.

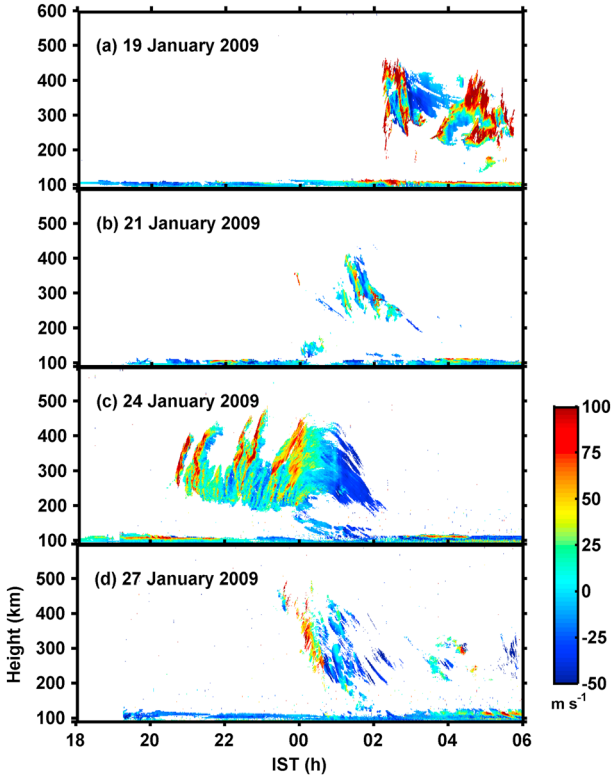

Figure 14. Height-time variations of line-of-sight velocities of the F region field-aligned irregularities observed at Gadanki on (a) 19 January, (b) 21 January, (c) 24 January and (d) 27 January 2009.

3.4. *F* Region Irregularities

Given the fact that the background zonal electric field underwent a negative excursion prior to the sunset, it would be interesting to examine to what extent these electric fields have affected the formation of *F* region irregularities. Moreover, since *F* region irregularities are known to occur in the postsunset hours during the December solstice and equinox of low solar activity conditions [*Chandra and Rastogi*, 1970], it would be interesting to examine the *F* region irregularities observed during the SSW period. For this purpose, we examine occurrence and nature of *F* region irregularities during 19–28 January based on ionosonde and radar observations. On these days, afternoon $\mathbf{E} \times \mathbf{B}$ drifts were either close to zero or downward. Signature of electric field reversal in ΔH data was observed from 23 January onward. Figure 12 shows spread *F* occurrence at Gadanki based on ionosonde observations made during 19–28 January. During 19–28 January, spread *F* was not observed on 20, 26, and 28 January. During this period, postmidnight- and frequency-type spread *F* was predominant, which are apparently different from those expected

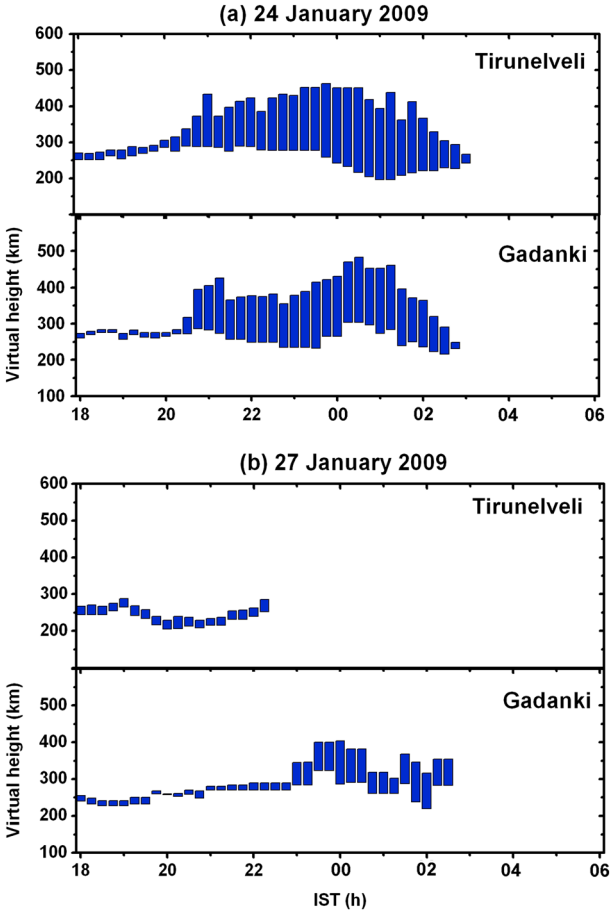

Figure 15. Ionosonde observations displaying the range spread *F* region echoes observed at (top) Tirunelveli and (bottom) Gadanki observed on (a) 24 January and (b) 27 January 2009. The vertical bar represents range spread (thickness of the echoing region) of the *F* region echoes and vertical bars having thickness >25 km represent spread *F*.

during January under low solar activity conditions [*Chandra and Rastogi*, 1970]. Range spread *F* was observed only on 21, 23, and 24 January. To characterize the *F* region irregularities further, radar observations from Gadanki on 19–25 and 27 are shown in Figures 13a–13h, respectively. Except for 24 January, radar echoes from *F* region FAI were observed during the postmidnight hours. Further, except on 19, 21, and 27 January, radar echoes were very weak and were observed in a narrow-height range and for short time. On the other hand on 24 January, not only the echoes were strong but also they occurred soon after sunset unlike on other nights. On this night, echoing regions can be characterized as plume structures, representing plasma bubbles. The last plume structure suddenly and rapidly descended soon after midnight, which subsequently weakened and disappeared.

To get some idea on the growth or decay phase of the irregularities, we present line-of-sight velocities of the irregularities on 19, 21, 24, and 27 January in Figures 14a–14d, respectively. These four nights are chosen since *F* region irregularities were considerably strong only on these nights. Usefulness of the velocities in interpreting the growth/decay phase lies on the assumption that in the growth phase the velocities are expected to be largely upward. On 24 January, irregularities commenced after the sunset and continued until ~02 IST in the postmidnight. The velocities were primarily upward before midnight and downward afterward. On other nights, irregularities commenced around/after midnight. Upward velocities were also observed on these nights, but surprisingly, large upward velocities were observed on 19 January, indicating the possible initiation of the irregularities in the postmidnight hours.

To gain further insight, it may be interesting to examine the contrasting events of 24 and 27 January, which occurred after the peak SSW activity. On both days, counterelectrojet and zonal electric field reversal were observed after 13 IST, but the counterelectrojet events turned back to normal by 18 IST. On 27 January, however, the counterelectrojet event was much stronger than that observed on 24 January. To understand the contrasting observations of 24 and 27 January, we consider ionosonde observations from Tirunelveli and Gadanki. Figure 15a (top and bottom) shows ionosonde observations, depicting the virtual height of the *F* layer and spread *F*, at Tirunelveli and Gadanki, respectively. The peak height of the *F* layer at the magnetic equator was 290 km prior to the occurrence of spread *F*. Range spread *F* was observed at both locations. They appeared almost at the same time (~20:30 IST) and disappeared at both places almost at the same time (03 IST). Also, no echo was detected at both places after 03 IST, presumably due to low plasma density.

Figure 15b (top and bottom) shows results of 27 January in the same way as those shown in Figure 15a. The peak *F* layer height at the magnetic equator was 250 km on this night and no spread *F* was observed until 22:15 IST, after which echoes disappeared. At Gadanki, spread *F* did not occur in the postsunset hours, but

weak spread *F* characterized with frequency spread *F* commenced around midnight hours (23:30 IST) at Gadanki. Again, on this night, no echo was detected after 03 IST.

4. Summary and Discussion

Ionospheric variations linked with the 2009 SSW observed in the Indian sector can be summarized as follows:

1. ΔH variations show counterelectrojet with clear semidiurnal variation in the electrojet. Occurrence of counterelectrojet after the onset of the SSW event show strong variation with periodicity of 15 days and relatively weak variation with periodicity of 6 days.
2. ΔH and $\mathbf{E} \times \mathbf{B}$ drift show a linear relation, and $\mathbf{E} \times \mathbf{B}$ drifts show large positive value in the morning and negative value in the afternoon, consistent with the semidiurnal variation in ΔH.
3. Remarkable changing patterns in the f_oF_2 and f_oF_3 were observed after the occurrence of SSW, and both f_oF_2 and f_oF_3 show strong 13–15 days periodicity and relatively weak 6–7 days periodicity after the onset of SSW event. In addition, f_oF_2 variations show 23 days periodicity just before the occurrence of SSW.
4. During the occurrence of counterelectrojet, E_{sq} disappeared, and corresponding to strong counterelectrojet events, there were no E_{sb}. A few case studies also suggest that E_{sb} was not formed at the off-equatorial location Gadanki, but *E* region plasma irregularities were observed by the ionosonde and radar with a close relationship between the two.
5. *F* region irregularities, except on 24 January, were observed in the postmidnight hours and were observed as weak radar echoes and weak-frequency spread *F*. On 24 January, irregularities were observed as multiple plume structures in radar maps and range spread *F*.

In addition to these, we have shown that during the Northern Hemisphere winter but during no-SSW period of December 2009, $\mathbf{E} \times \mathbf{B}$ drift and ΔH variations were very different from those observed during and after the SSW. During the non-SSW period, neither afternoon counterelectrojet nor negative $\mathbf{E} \times \mathbf{B}$ drifts were observed.

Occurrence of counterelectrojet and semidiurnal variation in ΔH linked with the 2009 SSW reported here are very much similar to those reported earlier [*Sridharan et al*., 2009; *Anderson and Araujo-Pradere*, 2010]. Although this linkage was originally suggested by *Stening* [1977], confirmation and detailed analysis on this linkage have come only in the recent past. It has been shown that counterelectrojet observed during the several past SSW events was linked with the enhancement of semidiurnal tide, and some of these were found to be lunar driven [e.g., *Stening et al*., 1996; *Rastogi*, 1999; *Sridharan et al*., 2009; *Fejer et al*., 2010; *Stening*, 2011]. As far as the 2009 SSW event is concerned, *Sathishkumar and Sridharan* [2013], analyzing magnetic field and mesospheric wind observed during the 2009 SSW from Tirunelveli, found that the counterelectrojet events were associated with the enhancement in the semidiurnal tide, and the large semidiurnal tide was mostly solar driven.

Coming to the $\mathbf{E} \times \mathbf{B}$ drift data presented here, we noted very similar behavior and a one-to-one relationship with ΔH. The one-to-one relationship between $\mathbf{E} \times \mathbf{B}$ drift and ΔH is promising for deriving zonal electric field, which we wish to take up in a future study. Although $\mathbf{E} \times \mathbf{B}$ drift data from Gadanki are limited, they are the first of their kind from Indian sector and are very much consistent with the finding of *Fejer et al*. [2010] based on vertical plasma drift from Jicamarca. Unusually large upward $\mathbf{E} \times \mathbf{B}$ drift in the morning and downward drift in the afternoon are consistent with those reported earlier from Jicamarca [*Chau et al*., 2009; *Fejer et al*., 2010]. Using Communication/Navigation Outage Forecasting System (C/NOFS) observations of $\mathbf{E} \times \mathbf{B}$ drift made during the 2009 SSW, *Rodrigues et al*. [2011] also found enhanced upward drift in the morning and downward drift in the afternoon. Although $\mathbf{E} \times \mathbf{B}$ drifts observed from different longitude sectors show unusually large upward drift in the morning hours and downward drift in the afternoon hours, such variations were found to have delayed occurrence in some longitude sectors [*Anderson and Araujo-Pradere*, 2010; *Fejer et al*., 2010]. Magnetic field observations during the January 1989 SSW event studied by *Rangarajan and Rastogi* [1989] also showed delayed response (earlier in the Indian sector than in the American sector). Occurrence of counterelectrojet as well as the reversal of zonal electric field in the afternoon linked with SSW has been observed worldwide, indicating that these two manifestations must be part of the global-scale wind system [*Stening et al*., 1996]. The wind system in this case must then be linked with SSW. During other periods also, counterelectrojet and reversal of zonal electric field have been observed. At those times, these two manifestations could be due to lunar tides [*Rastogi*, 1974] or local winds [*Raghavarao and Anandarao*, 1980].

As far as the SSW related local time change in the peak upward drift (i.e., shifting to earlier local time) is concerned, it has been attributed to the change in semidiurnal tide and lunar tide [*Fejer et al*., 2010; *Forbes and Zhang*, 2012; *Pedatella and Liu*, 2013]. Using the Whole Atmosphere Model (WAM), *Fang et al*. [2012] showed that the early occurrence of peak $\mathbf{E} \times \mathbf{B}$ drift is due to migrating tidal components. On the other hand, *Pedatella and Liu* [2013] showed that the phase shift of the westward propagating semidiurnal migrating tide is responsible for the increase in the vertical drift in the morning and decrease in the afternoon. *Fuller-Rowell et al*. [2010] also found similar results without including lunar tides in the WAM.

Having discussed the reversal of zonal electric field and occurrence of counterelectrojet, it may be relevant to discuss their effects on the behavior of *E* region. At the magnetic equator the observed disappearance of E_{sq} is consistent with the understanding on the formation of electrojet irregularities. A striking result, however, is the absence of dip equatorial E_{sb} corresponding to all days of strong counterelectrojet events. Earlier works on the occurrence of dip equatorial E_{sb} showed that they were closely related to counterelectrojet [e.g., *Devasia et al*., 2006]. At the off equatorial location, Gadanki, also we did not observe strong E_{sb} and strong radar echoes. Thus, the observations from Gadanki suggest the nonexistence of large wind shear (vertical shear in zonal wind) for the formation of strong E_{sb} and necessary driving forces for the generation of strong FAI. E_s, however, was observed at Gadanki with intermittent occurrence of weak E_{sb}, and a close relation between these and radar echoes was also found. Further, the occurrence of irregularities during the counterelectrojet events is in contrast with those observed at the equator. These observations suggest that wind shear capable of forming weak E_{sb} was present and the prevailing electron density gradient, electric field and/or neutral wind could generate plasma irregularities responsible for the radar echoes. At the geomagnetic equator, however, vertical shear of zonal wind is not effective for the formation of E_{sb}. *Reddy and Devasia* [1973] suggested that ion convergence along the magnetic field lines is possible if there is a horizontal shear in the horizontal wind. They predicted that such shears can be produced by short-period atmospheric gravity waves (AGWs), but the effectiveness of this mechanism depends on the characteristics of AGWs. The nonoccurrence of E_{sb} at Tirunelveli during the counterelectrojet period suggests either the nonexistence of driving force for the formation of E_{sb} [*Reddy and Devasia*, 1973; *Tsunoda*, 2008] or lack of equatorward transport mechanism of the intermittently occurring E_{sb} from off-equatorial location [*Reddy and Devasia*, 1973; *Chandra and Rastogi*, 1975]. Coming to the occurrence of E_{sb} and counterelectrojet, observationally, although a close relationship was found, it was not understood as to how the formation of E_{sb} is physically related to counterelectrojet. In the recent past, *Tsunoda* [2008] showed that the dynamical balance between horizontal wind and vertical polarization electric field in the *E* region sets up the anticorrelation between E_{sb} and electrojet strength and allows for the occurrence of E_{sb} over the dip equator under counterelectrojet conditions. Assuming that the proposed mechanism by *Tsunoda* [2008] links the E_{sb} and counterelectrojet, still it would be important to characterize the background conditions responsible for counterelectrojet during the SSW and non-SSW conditions. Observations of neutral winds and vertical electric field during counterelectrojet events associated with both SSW and non-SSW periods would be much useful to understand the underlying complex processes.

We also found noticeable 13–15 days periodicity in the occurrence of counterelectrojet, f_oF_2 and f_oF_3 after the commencement of the SSW. These can be related to quasi 16 day wave-induced variations widely reported in the literature. In addition, we also noted quasi 6 day periodicity in ΔH and f_oF_2. Quasi 16 day variation in f_oF_2 and f_oF_3 reported here are also consistent with zonal electric field variations observed in terms of ΔH. It may be mentioned here that simultaneous observations of $\mathbf{E} \times \mathbf{B}$ and ΔH showed a simple linear relationship between them, and hence, ΔH variations can be considered as a close proxy of zonal electric field variations. Further, a close linkage between the occurrence of F_3 layer and unusually large $\mathbf{E} \times \mathbf{B}$ drifts in the morning hours is noteworthy. Interestingly, f_oF_2 was also smaller than f_oF_3 during the morning hours, and a one-to-one anti-correlation between f_oF_2 and f_oF_3 was observed during the two spells of counterelectrojet period. These results are very much consistent with the understanding that upward $\mathbf{E} \times \mathbf{B}$ drift plays the primary role in the formation of F_3 layer. In fact, the effect of the large upward $\mathbf{E} \times \mathbf{B}$ drift was noted almost instantaneously, presumably due to its instantaneous role in lifting the F_2 layer to altitudes of low recombinational loss to form F_3 layer. A contrasting observation linked with westward electric field was also observed. Low values of f_oF_2 during 16–18 IST on several days around day numbers 60 and 75 were observed after about an hour of strong counterelectrojet events on those days. The counterelectrojet was linked with the reversal of the zonal

electric field (i.e., eastward to westward), which resulted in the descent of the *F* layer. Further, during 16–18 IST, production of ions decreases significantly. Thus, the reduced values of f_oF_2 can be attributed to the lack of production, and descent of the *F* layer to the recombination dominated lower altitudes.

Quasi 16 day variations in ΔH, total electron content (TEC), and f_oF_2 were also reported earlier from the Indian sector [*Vineeth et al*., 2009; *Sripathi and Bhattacharyya*, 2012; *Upadhayaya and Mahajan*, 2013]. Gravity wave-tidal interactions owing to enhanced activity in planetary scale waves resulting from the change in the lower atmospheric circulation linked with SSW has been proposed as the mechanism for strong quasi 16 day variation in the counterelectrojet [*Vineeth et al*., 2009], and the variations in TEC/f_oF_2 as well as electrojet are the manifestations of zonal electric fields [*Sripathi and Bhattacharyya*, 2012; *Upadhayaya and Mahajan*, 2013]. On the other hand *Park et al*. [2012] found pronounced 13 day modulation in electrojet strength in association with SSW, which they attributed to the enhancement of lunar tide in the ionosphere by the SSW effect. As the period of quasi 16 day modulation vary between 12 and 20 days, the amplification of lunar tide by the SSW as proposed by *Park et al*. [2012] becomes relevant. This attribute, however, needs to be ascertained through further research.

Coming to the 6 day periodicity in ΔH and f_oF_2, its amplitude is found to be weaker than that of 16 day. Further, although these variations were coincided with the period of afternoon counterelectrojet (and also afternoon reversal of zonal electric field), they were not observed at 16 IST (when counterelectrojet was in progress) in both data sets. It is important to mention that similar variations in ionospheric parameters have not been seen in other SSW events. Signature of similar periodicity in the ERA-Interim wind at 200 hPa (12 km) corresponding to the 2009 SSW has also been reported by *Sathishkumar and Sridharan* [2011], but it was observed only in meridional wind. *Sathishkumar and Sridharan* [2011] also analyzed f_oF_2 (based on Constellation Observing System for Meteorology, Ionosphere, and Climate (COSMIC) GPS radio occultation measurement), and magnetic field and mesospheric winds from Tirunelveli linked with this event, but they did not find such variations. While 6 day variations observed in ΔH and f_oF_2 indicate their linkages to zonal electric field variations, origin of such variations need to be investigated further.

Finally, one aspect that needs some discussion is the nature and time of occurrence of *F* region irregularities. Most of the irregularity events (except for 24 January) started occurring around/after midnight, and both ionosonde and radar observations indicate that the irregularities were weak in nature. Case studies based on 24 and 27 January observations showed that on 24 January, the equatorial *F* layer base was at a higher altitude (290 km) than that on 27 January (250 km). Moreover, on 27 January *F* layer started descending after 19 IST, which is adverse to the growth of the Rayleigh-Taylor (RT) instability. In this context, it may be important to mention that during the low solar activity condition, spread *F* was found to peak in the postmidnight hours in June solstice and in the postsunset hours in equinoxes and December solstice [*Chandra and Rastogi*, 1970]. Using radar observations made from Gadanki during the June solstice of low solar activity conditions of 2008, *Patra et al*. [2009] also found similar local time behavior displaying weak nature of the meter-scale irregularities responsible for radar echoes. This being the case, the predominance of postmidnight spread *F* and weak irregularities during January 2009 are apparently at variance with that reported by *Chandra and Rastogi* [1970]. It is quite likely that the tendency of spread *F* occurrence around or after midnight is related with the semidiurnal variation in the zonal electric field. The low altitude of the *F* layer and the westward electric field might have inhibited the growth of the RT instability soon after the sunset, but as time progressed, the rise of the *F* layer due to eastward electric field linked with the same semidiurnal behavior of zonal electric field might have engendered the growth of the RT instability manifesting delayed spread *F*. The low level of afternoon westward electric field on 24 January compared to that on 27 January seems to support this viewpoint. Note that on the evening of 27 January, the height of the *F* layer was close to 200 km, and *F* region irregularities did not occur then. We, however, noted premidnight height rise of the *F* layer on the same night, presumably due to eastward electric field linked with its semidiurnal behavior. Although the height of the *F* layer was below 300 km, the low ion-neutral collision frequency, owing to low plasma and neutral densities prevailing during the low solar activity condition of 2009, might have helped the growth of the RT instability even if the eastward electric field was not very high. In fact, *Stoneback et al*. [2011], using C/NOFS observations made during December 2008 to January 2009, found strong semidiurnal variation in the average $\mathbf{E} \times \mathbf{B}$ drift and concluded that such a variation could be responsible for upward drift near midnight, consistent with the postmidnight occurrence of *F* region irregularities reported here. Further studies are required to assess the role of SSW-related electric field effect on the occurrence of spread *F*.

5. Conclusions

We have presented variations in the low latitude ionospheric parameters in the Indian sector linked with the 2009 SSW. Among these **E** × **B** drift variations reported here are the first of their kind from the Indian sector as far as SSW is concerned. Results show strong semidiurnal variations in electrojet strength, Δ*H* and **E**× **B** drift with unusually large upward drift in the morning and downward drift in the afternoon and quasi 16 day variations in magnetic field, f_oF_2 and f_oF_3, which are consistent with those linked with other SSW events reported earlier. In addition, we found quasi 6 day periodicity in magnetic field and f_oF_2 variations, which need to be studied further. We have also presented new results on the possible effect of SSW-related neutral wind and electric field variations on the formation of low-latitude blanketing E_s and *E* and *F* region irregularities, not reported before. Given the fact that SSW has a strong impact on the neutral wind and electric field, their effects on the formation of plasma structures and irregularities are expected and need further investigations.

Acknowledgments

Authors gratefully thank the NARL and IIG technical staff for their efforts in making the observations reported here. P.P.C. gratefully acknowledges NARL for supporting his research through a Research Fellowship.

Alan Rodger thanks the reviewers for their assistance in evaluating this paper.

References

Anderson, D., and E. A. Araujo-Pradere (2010), Sudden stratospheric warming event signatures in daytime E × B drift velocities in the Peruvian and Philippine longitude sectors for January 2003 and 2004, *J. Geophys. Res.*, *115*, A00G05, doi:10.1029/2010JA015337.

Anderson, D. N., A. Anghel, K. Yumoto, M. Ishitsuka, and E. Kudeki (2002), Estimating daytime vertical E × B drift velocities in the equatorial F-region using ground-based magnetometer observations, *Geophys. Res. Lett.*, *29*(12), 1596, doi:10.1029/2001GL014562.

Axford, W. I. (1963), The formation and vertical movement of dense ionized layers in the ionosphere due to neutral wind shears, *J. Geophys. Res.*, *68*, 769–779, doi:10.1029/JZ068i003p00769.

Bhargava, B. N., and R. V. Subrahmanyan (1964), A study of blanketing sporadic E in the Indian equatorial region, *Proc. Indian Acad. Sci.*, *60*, 271–285.

Chandra, H., and R. G. Rastogi (1970), Solar cycle and seasonal variation of spread F near the magnetic equator, *J. Atmos. Terr. Phys.*, *32*, 439–443, doi:10.1016/0021-9169(70)90019-X.

Chandra, H., and R. G. Rastogi (1975), Blanketing sporadic E layer near the magnetic equator, *J. Geophys. Res.*, *80*, 149–153, doi:10.1029/JA080i001p00149.

Chau, J. L., B. G. Fejer, and L. P. Goncharenko (2009), Quiet variability of equatorial E × B drifts during a sudden stratospheric warming event, *Geophys. Res. Lett.*, *36*, L05101, doi:10.1029/2008GL036785.

Chau, J. L., N. A. Aponte, E. Cabassa, M. P. Sulzer, L. P. Goncharenko, and S. A. Gonzalez (2010), Quiet time ionospheric variability over Arecibo during sudden stratospheric warming events, *J. Geophys. Res.*, *115*, A00G06, doi:10.1029/2010JA015378.

Chau, J. L., L. P. Goncharenko, B. G. Fejer, and H.-L. Liu (2012), Equatorial and low latitude ionospheric effects during sudden stratospheric warming events, *Space Sci. Rev.*, *168*, 385–417, doi:10.1007/s11214-011-9797-5.

Devasia, C. V., N. Jyoti, K. S. V. Subbarao, D. Tiwari, C. Raghava Reddi, and R. Sridharan (2004), On the role of vertical electron density gradients in the generation of type II irregularities associated with blanketing Es (Esb) during counter equatorial electrojet events: A case study, *Radio Sci.*, *39*, RS3007, doi:10.1029/2002RS002725.

Devasia, C. V., V. Sreeja, and S. Ravindran (2006), Solar cycle dependent characteristics of the equatorial blanketing Es layers and associated irregularities, *Ann. Geophys.*, *24*, 2931–2947.

Fang, T.-W., T. Fuller-Rowell, R. Akmaev, F. Wu, H. Wang, and D. Anderson (2012), Longitudinal variation of ionospheric vertical drifts during the 2009 sudden stratospheric warming, *J. Geophys. Res.*, *117*, A03324, doi:10.1029/2011JA017348.

Fejer, B. G., M. E. Olson, J. L. Chau, C. Stoole, H. Luhr, L. P. Goncharenko, K. Yumoto, and T. Nagatsuma (2010), Lunar dependent equatorial ionospheric electrodynamic effects during sudden stratospheric warmings, *J. Geophys. Res.*, *115*, A00G03, doi:10.1029/2010JA015273.

Forbes, J. M., and X. Zhang (2012), Lunar tide amplification during January 2009 stratosphere warming event: Observations and theory, *J. Geophys. Res.*, *117*, A12312, doi:10.1029/2012JA017963.

Fuller-Rowell, T., F. Wu, R. A. Akmaev, T.-W. Fang, and E. A. Araujo-Pradere (2010), A whole atmosphere model simulation of the impact of a sudden stratospheric warming on thermosphere dynamics and electrodynamics, *J. Geophys. Res.*, *115*, A00G08, doi:10.1029/2010JA015524.

Goncharenko, L. P., and S. R. Zhang (2008), Ionospheric signatures of sudden stratospheric warming: Ion temperature at middle latitude, *Geophys. Res. Lett.*, *35*, L21103, doi:10.1029/2008GL035684.

Jin, H., Y. Miyoshi, D. Pancheva, P. Mukhtarov, H. Fujiwara, and H. Shinagawa (2012), Response of migrating tides to the stratospheric sudden warming in 2009 and their effects on the ionosphere studied by a whole atmosphere-ionosphere model GAIA with COSMIC and TIMED/SABER observations, *J. Geophys. Res.*, *117*, A10323, doi:10.1029/2012JA017650.

Kim, Y.-J., and M. Flatau (2010), Hindcasting the January 2009 arctic sudden stratospheric warming and its influence on the arctic oscillation with unified parameterization of orographic drag in NOGAPS. Part I: Extended-range stand-alone forecast, *Weather Forecast*, *25*, 1628–1644.

Liu, H., H. Jin, Y. Miyoshi, H. Fujiwara, and H. Shinagawa (2013), Upper atmosphere response to stratosphere sudden warming: Local time and height dependence simulated by GAIA model, *Geophys. Res. Lett.*, *40*, 635–640, doi:10.1002/grl.50146.

Manney, G. L., M. J. Schwartz, K. Kruger, M. L. Santee, S. Pawson, J. N. Lee, W. H. Daffer, R. A. Fuller, and N. J. Livesey (2009), Aura Microwave Limb Sounder observations of dynamics and transport during the record-breaking 2009 arctic stratospheric major warming, *Geophys. Res. Lett.*, *36*, L12815, doi:10.1029/2009GL038586.

Matsuno, T. (1971), A dynamical model of the stratospheric sudden warming, *J. Atmos. Sci.*, *28*, 1479–1494.

Maute, A., M. E. Hagan, A. D. Richmond, and R. G. Roble (2014), TIME-GCM study of the ionospheric equatorial vertical drift changes during the 2006 stratospheric sudden warming, *J. Geophys. Res. Space Physics*, *119*, 1287–1305, doi:10.1002/2013JA019490.

Park, J., H. Luhr, M. Kunze, B. G. Fejer, and K. W. Min (2012), Effect of sudden stratospheric warming on lunar tidal modulation of the equatorial electrojet, *J. Geophys. Res.*, *117*, A03306, doi:10.1029/2011JA017351.

Patra, A. K., D. V. Phanikumar, and T. K. Pant (2009), Gadanki radar observations of F region field-aligned irregularities during June solstice of solar minimum: First results and preliminary analysis, *J. Geophys. Res.*, *114*, A12305, doi:10.1029/2009JA014437.

Patra, A. K., P. P. Chaitanya, N. Mizutani, Y. Otsuka, T. Yokoyama, and M. Yamamoto (2012), A comparative study of equatorial daytime vertical E × B drift in the Indian and Indonesian sectors based on 150 km echoes, *J. Geophys. Res.*, *117*, A11312, doi:10.1029/2012JA018053.

Pedatella, N. M., and H. Liu (2013), The influence of atmospheric tide and planetary wave variability during sudden stratosphere warmings on the low latitude ionosphere, *J. Geophys. Res. Space Physics*, *118*, 5333–5347, doi:10.1002/jgra.50492.

Raghavarao, R., and B. G. Anandarao (1980), Vertical winds as a plausible cause for equatorial counter electrojet, *Geophys. Res. Lett.*, *7*, 357–360.

Rangarajan, G. K., and R. G. Rastogi (1989), Longitudinal difference in magnetic field variations associated with quiet day counter electrojet, *J. Geomagn. Geoelectr.*, *45*, 649–656.

Rastogi, R. G. (1972), Sudden disappearance of Esq and the reversal of the equatorial electric fields, *Ann. Geophys.*, *28*, 717–728.

Rastogi, R. G. (1974), Lunar effects in the counter-electrojet near the magnetic equator, *J. Atmos. Terr. Phys.*, *56*, 167–170.

Rastogi, R. G. (1999), Morphological aspects of a new type of counter electrojet event, *Ann. Geophys.*, *17*, 210–219, doi:10.1007/s00585-999-0210-6.

Rastogi, R. G., and J. A. Klobuchar (1990), Ionospheric electron content within the equatorial F_2 layer anomaly belt, *J. Geophys. Res.*, *95*, 19,045–19,052.

Reddy, C. A., and C. V. Devasia (1973), Formation of blanketing sporadic E layers at the magnetic equator due to horizontal wind shears, *Planet. Space Sci.*, *21*, 8111–817.

Rodrigues, F. S., G. Crowley, S. M. I. Azeem, and R. A. Heelis (2011), C/NOFS observations of the equatorial ionospheric electric field response to the 2009 major sudden stratospheric warming event, *J. Geophys. Res.*, *116*, A09316, doi:10.1029/2011JA016660.

Sathishkumar, S., and S. Sridharan (2009), Planetary and gravity waves in the mesosphere and lower thermosphere region over Tirunelveli (8.7°N, 77.8°E) during stratospheric warming events, *Geophys. Res. Lett.*, *36*, L07806, doi:10.1029/2008GL037081.

Sathishkumar, S., and S. Sridharan (2011), Observations of 2-4 day inertia-gravity waves from the equatorial troposphere to the F region during the sudden stratospheric warming event of 2009, *J. Geophys. Res.*, *116*, A12320, doi:10.1029/2011JA017096.

Sathishkumar, S., and S. Sridharan (2013), Lunar and solar tidal variabilities in mesospheric winds and EEJ strength over Tirunelveli (8.7°N, 77.8°E) during the 2009 major stratospheric warming, *J. Geophys. Res. Space Physics*, *118*, 533–541, doi:10.1029/2012JA018236.

Sridharan, S., S. Sathishkumar, and S. Gurubaran (2009), Variabilities of mesospheric tides and equatorial electrojet strength during major stratospheric warming events, *Ann. Geophys.*, *27*, 4125–4130.

Sripathi, S., and A. Bhattacharyya (2012), Quiet time variability of the GPS TEC and EEJ strength over Indian region associated with major sudden stratospheric warming events during 2005/2006, *J. Geophys. Res.*, *117*, A05305, doi:10.1029/2011JA017103.

Stening, R. J. (1977), Electron density changes associated with the equatorial electrojet, *J. Atmos. Terr. Phys.*, *39*, 157–164, doi:10.1016/0021-9169(77)90109-X.

Stening, R. J. (2011), Lunar tide in the equatorial electrojet in relation to stratospheric warmings, *J. Geophys. Res.*, *116*, A12315, doi:10.1029/2011JA017047.

Stening, R. J., C. E. Meek, and A. H. Manson (1996), Upper atmosphere wind systems during reverse equatorial electrojet events, *Geophys. Res. Lett.*, *23*, 3243–3246.

Stoneback, R. A., R. A. Heelis, A. G. Burrell, W. R. Coley, B. G. Fejer, and E. Pacheco (2011), Observations of quiet time vertical drift in the equatorial ionosphere during the solar minimum period of 2009, *J. Geophys. Res.*, *116*, A12327, doi:10.1029/2011JA016712.

Tsunoda, R. T. (2008), On blanketing sporadic E and polarization effects near the equatorial electrojet, *J. Geophys. Res.*, *113*, A09304, doi:10.1029/2008JA013158.

Upadhayaya, A. K., and K. K. Mahajan (2013), Ionospheric F_2 region: Variability and sudden stratospheric warming, *J. Geophys. Res. Space Physics*, *118*, 6736–6750, doi:10.1002/jgra.50570.

Vineeth, C., T. K. Pant, and R. Sridharan (2009), Equatorial counter electrojets and polar stratospheric sudden warmings—A classical example of high latitude-low latitude coupling?, *Ann. Geophys.*, *27*, 3147–3153.

Wang, H., T. J. Fuller-Rowell, R. A. Akmaev, M. Hu, D. T. Kleist, and M. D. Iredell (2011), First simulations with a whole atmosphere data assimilation and forecast system, *J. Geophys. Res.*, *116*, doi:10.1029/2011JA017081.